Phys Chem Minerals (2006) 33:655–666
DOI 10.1007/s00269-006-0120-z

ORIGINAL PAPER

DFT study of the cation arrangements in the octahedral and tetrahedral sheets of dioctahedral 2:1 phyllosilicates

Alfonso Hernández-Laguna · Elizabeth Escamilla-Roa · Vicente Timón · Martin T. Dove · C. Ignacio Sainz-Díaz

Received: 7 April 2006 / Accepted: 4 September 2006 / Published online: 25 October 2006

Abstract Quantum mechanical calculations based on the density functional theory (DFT) are used to study the crystal structures of dioctahedral 2:1 phyllosilicates. The isomorphous cation substitution is investigated by exploring different substitutions of octahedral Al^{3+} by Mg^{2+} or Fe^{3+}, tetrahedral substitution of Si^{4+} by Al^{3+}, and different interlayer cations (IC) (Na^{+}, K^{+}, Ca^{2+}, and Mg^{2+}). Samples with different kinds of layer charges are studied: only tetrahedrally charged, only octahedrally charged, or mixed octahedral/tetrahedral charged. The effect of the relative arrangements of these substitutions on the lattice parameters and total energy is studied. The experimental observation of segregation tendency of Fe^{3+} and dispersion tendency of Mg^{2+} in the octahedral sheet is reproduced and explained with reference to the relative energies of the octahedral cation arrangements. These energies are higher than those due to the IC/tetrahedral and IC/octahedral relative arrangements. The tetrahedral and octahedral substitutions that generate charged layers also tend to be dispersed. The octahedral cation exchange potentials change with the IC-charge/ionic radius value.

A. Hernández-Laguna · E. Escamilla-Roa · V. Timón
Estación Experimental del Zaidín,
Consejo Superior de Investigaciones Científicas (CSIC),
C/ Profesor Albareda 1, Granada 18008, Spain

M. T. Dove
Department of Earth Sciences, University of Cambridge,
Downing Street, Cambridge CB2 3EQ, UK

C. Ignacio Sainz-Díaz (✉)
Instituto Andaluz de Ciencias de la Tierra,
Consejo Superior de Investigaciones Científicas (CSIC)/
Universidad de Granada, Av. Fuentenueva s/n,
Granada 18002, Spain
e-mail: sainz@lec.ugr.es

Introduction

A wide diversity of 2:1 phyllosilicates exists in nature because these materials can accommodate a wide range of cation compositions in the octahedral and tetrahedral sheets. In dioctahedral 2:1 phyllosilicates, isomorphous substitution of Al^{3+} by Fe^{3+} or Mg^{2+} in the octahedral sheet, or Si^{4+} by Al^{3+} in the tetrahedral sheet, can result in a net negative charge that is balanced by the presence of cations in the interlayer space. Each sheet can have different cation arrangements, and different layers can coexist within the same crystal leading to the formation of a mixed-layer structure. Hence the determination of the arrangement of cations within the sheets is a complex problem. Nevertheless, this type of study can be useful to understand natural processes, such as the smectite to illite transformation, and to analyse how cation arrangements affect lattice stability. Understanding the mechanism of the smecite/illite transformation is important for a number of reasons, not least because the illite/smectite distribution can be used as a proxy in the exploration of underground oil deposits (Velde and Espitalié 1989). Furthermore, the stability of the clay barriers for toxic and nuclear waste disposal is closely related to the smectite–illite transformation, changing the cation exchange and water swelling capacity, and thereby increasing the risk of leaks in the barrier

(Krauskopf 1991). Finally, there are many industrial applications of smectite due to its catalytic and adsorptive properties (Güven 1988); for example, the cation exchange capacity of these minerals can be very useful to remove contaminant soluble cations in natural media (Meunier 2005).

The phenomenon of cation ordering in aluminosilicate minerals is one of the important subjects in modern structural mineral sciences, particularly since it can have a significant effect on the thermodynamic properties of materials. The cation arrangements within the octahedral sheet of phyllosilicates have been studied experimentally. Besson et al. (1987) found from infrared (IR) studies that octahedral cation arrangements are not random at all, but Al^{3+} and Fe^{3+} cations tend to segregate from each other. Using ^{27}Al nuclear magnetic resonance (NMR) on montmorillonite, Morris et al. (1990) found that Fe was either segregated from Al in the octahedral sheet or present in a phase different from smectite. Schroeder (1993) studied shale illite–smectite (I–S) samples using ^{27}Al NMR and found that Fe mixes with Al in samples with low Fe content, but also that Fe segregates from Al in Fe-rich specimens. Drits et al. (1997) studied the isomorphous cation arrangement by IR, Mössbauer, and extended X-ray absorption fine structure (EXAFS) spectroscopy in celadonites, glauconites, and Fe-illites, finding certain short-range ordering. Muller et al. (1997) studied octahedral cation arrangement of the Camp–Bertaux montmorillonite using X-ray diffraction (XRD), EXAFS, and Fourier-transformed infrared (FT-IR) spectroscopy, and observed that Mg and Fe form clusters that segregate from Al. FT-IR and ^{27}Al NMR spectroscopic studies and Reverse Monte Carlo (RMC) simulations on illite/smectite samples showed a short-range ordering in the octahedral cations with a tendency to be segregated for Fe^{3+} cations and to be dispersed for Mg^{2+} cations (Cuadros et al. 1999; Sainz-Díaz et al. 2001a). Though most of the papers agree with the Fe^{3+} segregation in clusters of the other cations, no definitive conclusion can be extracted from this experimental work.

Monte Carlo simulations have been carried out on the order–disorder behaviour of the tetrahedral sheet (Al/Si) in micas (Herrero et al. 1987; Herrero and Sanz 1991; Palin et al. 2001), the tetrahedral (Al/Si) and octahedral (Al/Mg) sheets in phengite (Palin et al. 2003), and the octahedral sheet in illites and smectites with respect to two-species systems Al/Fe, Al/Mg, Fe/Mg and three-species systems Al/Fe/Mg (Sainz-Díaz et al. 2003a, b). In each case, the simulations were able to reproduce experimental results where available. All these previous studies were based on calculations with empirical interatomic potentials. In this work, we extend this line of research by applying quantum mechanical methods for the calculations of the energetics of cation arrangements, considering the relative arrangements of tetrahedral, octahedral, and interlayer cations simultaneously. This work predicts a short-range cation ordering that is consistent with experimental results.

Models and methods

We perform ab initio total energy calculations using the numerical atomic orbital (NAO) methodology implemented in the density functional theory SIESTA program (Artacho et al. 1999; Soler et al. 2002). We use the generalized gradient approximation (GGA) and the Perdew–Burke–Ernzerhof parameterization (Perdew et al. 1996) of the exchange–correlation functional. A uniform mesh with certain plane-wave cut-off energy is used to represent the electron density, the local part of the pseudopotential and the Hartree and exchange–correlation potentials. Core electrons are replaced by norm-conserving pseudopotentials (Troullier and Martins 1991) factorized in the Kleinman–Bylander form (Kleinman and Bylander 1982), including scalar-relativistic effects (Bachelet and Schluter 1982), and nonlinear partial-core corrections (Louie et al. 1982) in the K and Fe cases.

The basis sets are made of strictly localized numerical atomic orbitals (NAOs). Their localization cut-off radii correspond to an energy shift of 270 meV (Artacho et al. 1999). The basis set used in this work is double-ζ polarized (DZP) following the perturbative polarization scheme (Artacho et al. 1999). Preliminary calculations were performed exploring different calculation parameters (Sainz-Díaz et al. 2005) and DZP calculations were considered valid based on our comparative studies. The geometrical features obtained with mesh cut-off energy of 150 Ry and a k-grid cut-off of 5 Å were close to experiment. Higher values of these parameters do not yield significant differences in geometrical features of our samples. In each structure, we relax all atomic positions and lattice parameters using the conjugated gradient minimization method, with a force tolerance of 0.04 eV/Å.

Experimental atomic coordinates for the crystal structure of smectites and illites are taken from the models proposed by Tsipursky and Drits (1984) based on oblique-texture electron diffraction studies of di-octahedral smectites. The H atom coordinates are taken from the previous study of Giese (1979) and were

optimised previously by means of interatomic empirical potential calculations (Sainz-Díaz et al. 2001b). All samples are trans-vacant, and completely dry in our simulations. We use only one unit cell (40–43 atoms) with periodic boundary conditions; these conditions obviously lead to high substitution levels and highly ordered structures. It is well known that isomorphic substitutions in 2:1 dioctahedral phyllosilicates do not show any long-range order (Sainz-Díaz et al. 2003a), but it is probable that our models might be found in small-localized domains in natural samples. Hence these models can be useful to give a first insight into how the isomorphic substitution behaves in these minerals at this higher level of theory. Further calculations using larger supercells are now in progress in order to explore more arrangements.

Different cation substitutions of Si^{4+} by Al^{3+} in the tetrahedral sheet, and Al^{3+} by Mg^{2+} and Fe^{3+} in the octahedra sheet are considered, and, in order to neutralize the layer charge coming from the isomorphic substitution, Na^+, K^+, Ca^{2+}, and Mg^{2+} are considered as interlayer cations. In total, 18 samples have been constructed (Table 1). In this series, there are samples without tetrahedral charge, samples with a certain tetrahedral charge, samples without octahedral charge (end member of beidellite), and samples with high octahedral charge. Samples with a very high Fe content in the octahedral sheet are also included. Charged samples have integer values of the charge in a unit cell with $I_{x+y}(Al_{4-x-z}Mg_xFe^{3+}{}_z)(Si_{8-y}Al_y)O_{20}(OH)_4$, where I represents the interlayer cation.

Table 1 Chemical composition of the samples studied

Sample	Si^{4+} (T)	Al^{3+} (T)	Al^{3+} (Oc)	Mg^{2+} (Oc)	Fe^{3+} (Oc)	Interlayer cation
S1	7	1	4			Na^+
S2	7	1	2		2	Na^+
S3	8		2	2		$2Na^+$
S4	8		3	1		Na^+
S5	8		2	1	1	Na^+
S6	7	1	3		1	Na^+
S7	7	1	4			K^+
S8	7	1	2		2	K^+
S9	8		2	2		$2K^+$
S10	8		3	1		K^+
S11	8		2	1	1	K^+
S12	7	1	3		1	K^+
S13	7	1	3	1		Mg^{2+}
S14	7	1	3	1		Ca^{2+}
S15	8		2	2		Ca^{2+}
S16	7	1	3	1		$2K^+$
S17	7	1	3	1		$2Na^+$
S18	8		2	2		Mg^{2+}

T tetrahedral, *Oc* octahedral

Structural formulae on the basis of O_{20} $(OH)_4$

These cation substitutions decrease the symmetry of the crystal structure, and different cation arrangements can exist for a certain cation composition. For example, a simple tetrahedral substitution of $^{IV}Al^{3+}$ per unit cell generates the presence of one monovalent interlayer cation (IC) per unit cell. This $^{IV}Al^{3+}$ substitution can be in two possible relative positions with respect to the IC (Fig. 1a, b). A specific definition of the cation substitution sites should be established for the comparison of different cation arrangements. Considering a projection of these lattice structures on the (001) plane, the tetrahedral Al^{3+} cation can be close to the (100) plane (T1) or close to the (200) plane (T2) (Fig. 1), and also the octahedral cation substitution can be close to the (100) plane (O1) or close to the (200) plane (O2) (Fig. 2). In addition, two different relative cation arrangements can be considered in the O2/T2 forms, with simultaneous tetrahedral and octahedral cation substitutions, the O2–T2 (Fig. 1b) and O2–T2a (Fig. 1c) arrangements. We explore several cation substitution arrangements within the same composition in order to determine the energy and geometrical differences between them (Tables 2, 3).

Results

Atomic positions of the optimised crystal structures are described elsewhere (for more details see the Supplementary Material of Sainz-Díaz et al. 2002). Our calculations reproduce well the experimental values of crystal lattice parameters taken from experimental models (Tsipursky and Drits 1984; Sato et al. 1992) for these clay minerals, although the calculated values of the *a* parameter are slightly higher than the experimental one (Table 2) (Sainz-Díaz et al. 2002).

Samples with monosubstitution of cations

The samples with only one tetrahedral substitution of Al^{3+} (^{IV}Al) per unit cell, and no octahedral substitution, (S1 and S7) can have two possible relative cation arrangements (T1 and T2) between ^{IV}Al and the interlayer cation (IC) (see Fig. 1a, b for the T1 and T2 cation arrangements, respectively). The sodium (S1) and potassium (S7) samples have similar lattice parameters with slight differences. The *a*, *b*, and *c* parameters are slightly larger in S7 than in S1. However, the size difference between both IC is larger than the distorsion that they introduce in the lattice parameters. This fact has been highlighted by Rosso et al. (2001) by means of ab initio calculations on the exchange of K^+ and Cs^+ as the IC in mica models. They

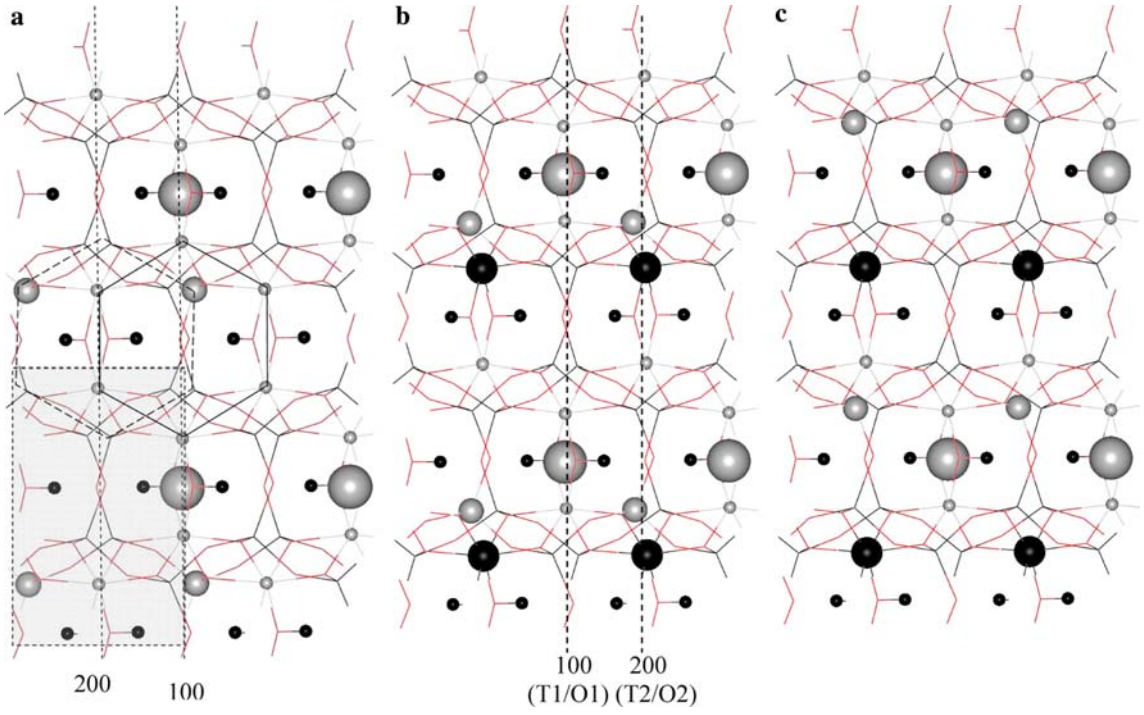

Fig. 1 Relative cation arrangements, T1 (**a**), T2 (**b**), and T2a (**c**), between the IC and ^{IV}Al for studied samples. Tetrahedral substitution on the plane close to (*i*00) is named T*i*, and octahedral substitutions close to the (*i*00) plane are named O*i*. The octahedral Al and ^{IV}Al cations and IC are represented by *small, medium, and large grey balls* respectively; octahedral substitution cations (Fe $^{3+}$ and Mg^{2+} in O2 arrangement) and H atoms are represented by *medium and small black balls*, respectively. The unit cell used in the calculations is marked with a *shadowed square*. The hexagons that are formed by tetrahedral and octahedral cations are marked by *dashed and plain lines*, respectively. *Vertical dashed lines* represent the (200) and (100) planes. This model can represent the S1 and S7 samples (without octahedral substitution), S4 and S10 samples (without $^{IV}Al^{3+}$), and S6, S12-S14 samples (where the octahedral substitution can be Mg^{2+} or Fe^{3+}, and IC can be Na^{+}, K^{+}, Ca^{2+}, or Mg^{2+})

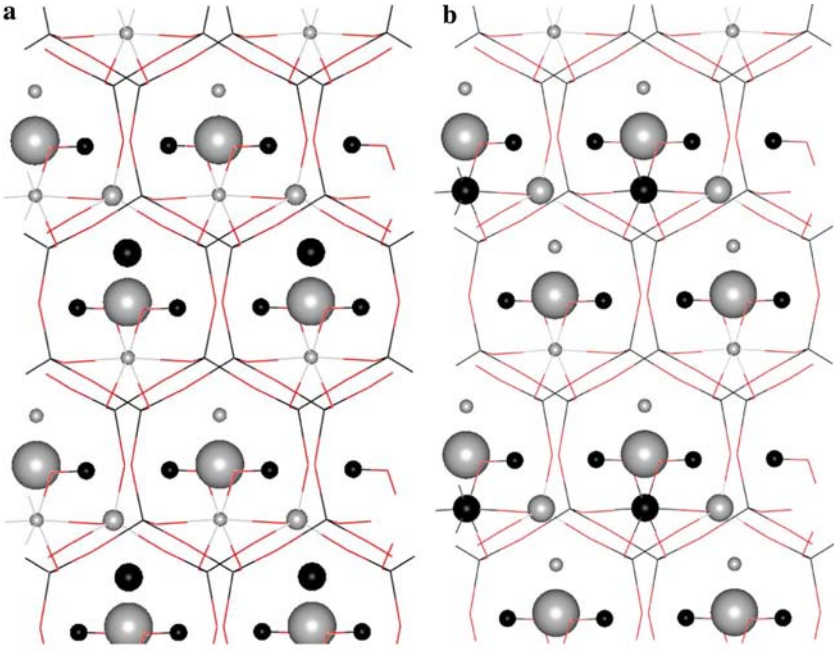

Fig. 2 Relative arrangements, O2 (**a**) and O1 (**b**), between the IC and octahedral substitution for octahedrically monosubstituted samples. The octahedral Al and ^{IV}Al cations, and IC are represented by *small, medium, and large grey balls* respectively and octahedral substitution and H atoms are represented by *medium and small black balls*, respectively. The $^{IV}Al^{3+}$ is in T2 arrangement. This model can represent the S16 and S17 samples, S4 and S10 samples (with only half of the IC sites occupied)

Table 2 Lattice parameters (distances in Å, angles in degrees) and relative energy of the cation arrangements calculated and experimental values (Tsipursky and Drits 1984; Sato et al. 1992)

Sample	ΔE (eV)	a	b	c	β	$c\sin\beta$
Exp		5.18	8.97–9.01	10.05–10.2	99.5–101.4	9.8–9.99
S1 T1	0.0	5.25	9.10	10.08	102.1	9.86
S1 T2	0.0017	5.26	9.00	10.05	101.9	9.83
S7 T1	0.0	5.27	9.14	10.20	102.6	9.95
S7 T2	0.0081	5.29	9.12	10.12	102.1	9.90
S4 O2	0.0	5.27	9.12	10.07	103.0	9.81
S4 O1	0.0082	5.28	9.13	10.16	105.3	9.80
S10 O2	0.0	5.29	9.16	10.08	102.5	9.84
S10 O1	0.0257	5.30	9.16	10.06	102.3	9.83
S6 O1T2	0.0	5.25	9.05	10.07	102.9	9.82
S6 O2T2	0.0606	5.25	9.05	10.05	102.5	9.81
S12 O1T2	0.0	5.27	9.07	10.19	102.8	9.94
S12 O2T2	0.0454	5.27	9.08	10.18	102.7	9.93
S13 O2T2a	–0.6215	5.32	9.12	9.64	96.8	9.57
S13 O1T2	0.0	5.28	9.18	10.17	105.7	9.79
S13 O2T2	0.0094	5.28	9.17	10.14	105.5	9.77
S14 O2T2	0.0	5.29	9.10	10.03	102.7	9.78
S14 O1T2	0.0347	5.30	9.09	10.07	103.8	9.78
S14 O2T2a	–0.3559	5.29	9.10	10.02	102.6	9.78
S16 O1T2	0.0	5.29	9.17	10.21	102.1	9.98
S16 O2T2	0.0163	5.29	9.17	10.21	102.1	9.98
S16 O2 T2a	–0.3359	5.29	9.17	10.23	102.1	10.00
S17 O1T2	0.0	5.27	9.13	10.11	102.0	9.89
S17 O2T2	0.0171	5.25	9.13	10.10	101.8	9.89
S17 O2T2a	–0.325	5.26	9.12	10.10	101.8	9.89

Table 3 Lattice parameters (distances in Å, angles in degrees) and relative energy of the cation arrangements calculated for samples octahedrally bisubstituted (o, m, and p, mean *ortho*, *meta* and *para*, respectively) and experimental values (Tsipursky and Drits 1984; Sato et al. 1992)

Sample	ΔE (eV)	a	b	c	β	$c\sin\beta$
Exp		5.18	8.97–9.01	10.05–10.2	99.5–101.4	9.8–9.99
S3m	0.0	5.26	9.10	9.99	101.6	9.79
S3p	0.2301	5.25	9.12	10.06	101.9	9.84
S3o	0.5681	5.26	9.10	9.98	101.6	9.78
S9m	0.0	5.28	9.15	10.07	101.8	9.86
S9p	0.2907	5.30	9.15	10.08	101.5	9.88
S9o	0.6097	5.27	9.15	10.08	101.6	9.87
S15m	0.0	5.29	9.11	9.95	103.1	9.69
S15p	0.1423	5.28	9.09	10.02	104.2	9.71
S15o	0.6178	5.27	9.11	9.96	102.4	9.73
S18p	0.0	5.20	9.10	10.06	109.9	9.46
S18o	0.7600	5.26	9.09	10.00	109.4	9.43
S18m	0.9653	5.15	8.91	9.66	101.6	9.46
S5m	0.0	5.26	9.08	10.01	102.6	9.77
S5p	0.0077	5.27	9.08	10.05	103.3	9.78
S5o	0.3645	5.26	9.09	10.0	102.9	9.75
S11m	0.0	5.29	9.14	10.05	102.7	9.80
S11p	0.0359	5.29	9.12	10.08	103.0	9.82
S11o	0.3109	5.28	9.15	10.03	102.5	9.79
S2o	0.0	5.25	9.01	10.06	103.5	9.78
S2p	0.1192	5.25	9.03	10.03	102.3	9.80
S2m	0.22	5.24	9.02	10.02	102.2	9.79
S8o	0.0	5.27	9.08	10.11	102.6	9.87
S8p	0.1101	5.27	9.07	10.16	102.1	9.93
S8m	0.2319	5.27	9.06	10.13	102.5	9.89

concluded that the difference in the interlayer space appears to be insensitive to the size of IC. If we take the effective ionic radius (ir) for octahedral coordination as a suitable measure (Shannon 1976), we find that Na^+ and K^+ cations show differences of 0.36 Å in the ir, while the *c* parameter increases by only 1/8 of the ionic diameter differences. Let us consider the projection of the *c* axis over the perpendicular to the (001) plane, $c\sin\beta$, (Table 2), that is related to the opening of the interlayer space. The average value of this quantity increases by only 0.08 Å, lower still than the changes in the *c* value. Basal oxygens of the tetrahedral sheet form a network of triangles joined by the vertices that draw another hexagonal network at the surface of the interlayer space. The IC is located in the hole formed in the centre of these hexagons. The distortion produced by the coupling of the tetrahedral and octahedral sheets means that these hexagons change from a hexagonal symmetry to a ditrigonal symmetry with a certain angular freedom. The angles of the basal oxygens of the tetrahedra at ditrigonal hole can change by the presence of the IC in such a way that a different hole size may be found for different IC. The arrangement T2 has values of the *a* lattice parameter a little higher than in T1, but T1 has values of the *b*, *c*, β, and $c\sin\beta$ *lattice* parameters a little higher than in T2 (Table 2). Smaller differences are found between the other parameters in arrangements T1 and T2 (Table 2). In both samples, the arrangement T1 is energetically more stable than T2, but the differences are very small. The difference in energy between the T2 and T1 arrangements is higher in S7 than in S1, due again to the higher ionic radius of K^+ than Na^+, and the interaction of the IC with $^{IV}Al^{3+}$ will also be higher in S7 than in S1.

Samples with only one octahedral cation substitution (Mg^{2+}) per unit cell and no tetrahedral substitution (S4 and S10) can also have two possible arrangements, O1 and O2, of Mg^{2+} with respect to IC (see Fig. 2a, b for the O2 and O1 cation arrangements, respectively). The *a* and *b* lattice parameters of both arrangements of each sample have the same behaviour with respect to the IC, Na^+ (S4) and K^+ (S10), as the S1 and S7 samples. The *a* and *b* parameters are slightly higher in S10 than in S4. The $c\sin\beta$ value is slightly higher in S10 than in S4 but the difference is much lower here than between S7 and S1 (Table 2). Besides, $c\sin\beta$ is shorter in S4/S10 samples than in S1/S7. This could possibly be caused by the octahedral source of negative charges created by the isomorphic substitution that is more distributed in the inner apical tetrahedral oxygens and attracts to the IC from both sides of the interlayer space, whereas in S1 and S7 the charge defect comes from the external basal tetrahedral sheet of only one side of the interlayer space. Similar effect was detected experimentally by Sato et al. (1992) in montmorillonite and beidellite with Na^+ and K^+ as IC.

The lattice parameters are similar in both arrangements, O1 and O2 (Table 2), with the exception of *c* and β in S4–O1, which are larger than those in O2. In S4 and S10, O2 is more stable than O1 with an energy difference slightly higher than in the series with only tetrahedral substitution (S1, S7). The lower stability of O1 can be due to the polyhedron distortion and the stronger repulsion between the IC and Mg^{2+} in O1 where both cations are closer than in O2. This interaction difference will be higher here than in S1/S7 group due to the shorter $c\sin\beta$ values, whereas in S1/S7 group this energy can be partially absorbed by tilting of tetrahedrons.

Samples with simultaneous two-substitutions in octahedral and tetrahedral sheets

Samples, with only one $^{IV}Al^{3+}$ per unit cell as in S1 and S7, can have another octahedral cation substitution per unit cell; the most common example is $^{VI}Fe^{3+}$, which does not create an additional octahedral charge (S6 and S12). Keeping the tetrahedral substitution in T2 constant, two possible cation arrangements can be considered for the $^{VI}Fe^{3+}$ cation with respect to the IC, both of which are the same as in S4 and S10: O1 and O2 (Fig. 2a, b for the O2 and O1 cation arrangements, respectively). No significant differences in the values of the lattice parameters are observed between both arrangements (Table 2). The $c\sin\beta$ values of S6 are similar to S4. However, S12 shows higher *c* and $c\sin\beta$ values than S6 due to the presence of K^+ as IC in the same way as in previous samples. In both cases, O1 is more stable than O2, unlike the previous samples; this is possibly because of the lack of charge in the octahedral sheet. However, in the less stable arrangement, O2, the tetrahedral and octahedral substitutions are very close in the 200 plane projection, whereas in O1 the octahedral substitutions are half way between two $^{IV}Al^{3+}$. Hence the interactions between $^{IV}Al^{3+}$ and $^{VI}Fe^{3+}$ mean that the difference of energy between both arrangements is greater than in previous samples, 0.06 eV (1.4 kcal/mol).

Cation substitutions can produce octahedral and tetrahedral charge simultaneously, with one $^{IV}Al^{3+}$ and one Mg^{2+} cation per unit cell, respectively (S13, S14, S16, and S17). These samples have different IC, namely, Mg^{2+}, Ca^{2+}, K^+, and Na^+ for S13, S14, S16, and S17, respectively. Three possible cation arrangements can be considered: two for the octahedral Mg^{2+} with

respect to the IC which keep the tetrahedral arrangement constant in T2, O1, and O2 (Figs. 1b, 2), and one additional arrangement T2a where the tetrahedral substitution is close to the plane (200) but in a different hexagonal ring of tetrahedra from where the IC is located (Fig. 1c). No new significant lattice parameter difference was observed between the optimised arrangements, except in the O2T2a arrangement of S13. This last arrangement shows all lattice parameters to be different from those of the rest of S13 arrangements and other samples of this group. This is due to the existence of a different polymorph with a clearly low value of β. Possibly, the high charge/radius ratio of Mg^{2+}, as IC, may be the main reason of this polymorphism. This phenomenon is different to cation substitution arrangement effect in our samples and it should be explored separately. Further calculations in this way will be performed in order to explain this phenomenon.

In this series where IC charges are different, the charge/ionic-radius (q/ir) ratio can be correlated with the deviation of $c\sin\beta$ from that of pyrophyllite, $c\sin\beta - (c\sin\beta)_{pyro}$, taking average values in these samples (Fig. 3). A negative linear relationship is found with a low slope according to previous results of Rosso et al. (2001). From this linear relationship we can suggest that the q/ir ratio may be a characteristic value in determining the spacing between layers because of the IC size.

In all samples of this series the O2T2a arrangement is the most stable (Table 2). In S13, the O1–T2 arrangement is more stable than O2–T2, whereas in S14 the O2 is more stable than O1. The higher ionic radius of Ca^{2+} than Mg^{2+} means that the repulsion between the IC and octahedral Mg^{2+} increases the energy of O1 in S14. In samples with a monovalent IC, S16, and S17, all tetrahedral cavities are occupied with IC and the interaction between IC and octahedral Mg^{2+} is similar for both arrangements (Fig. 2). In these last samples O1 is slightly more stable than O2. In the T2a arrangement, the $^{IV}Al^{3+}$ cation is in a different relative position with respect to the octahedral substitution cation, such that $^{IV}Al^{3+}$ is not as close to the Mg^{2+} as in T2, but is more or less equidistant between two Mg^{2+} along the direction of b axis (Fig. 1c). In this group, this arrangement of ^{IV}Al (T2a) is much more stable than T2, the energy difference being significantly higher than between previous arrangements.

Samples with two octahedral substitutions of Mg^{2+}

Two Mg^{2+} cations can substitute for two Al^{3+} per unit cell in the octahedral sheet (samples S3, S9, S15, and S18), generating a negative charge of 2 e^- per unit cell that is compensated by two Na^+ (S3), K^+ (S9), one Ca^{2+} (S15) or one Mg^{2+} (S18) as IC per unit cell (Table 3). In this group, no $^{IV}Al^{3+}$ is present and the tetrahedral sheet is homogeneous. These samples have an additional type of cation arrangement related to the octahedral substitution. Using an analogy to the hexagons of octahedral cations with the benzene ring, we can use the same nomenclature as the benzene substitutions. The *ortho*, *meta* and *para* arrangements will be those where both cation substitution sites in the unit cell are nearest neighbours, separated by one Al^{3+}, or separated by two Al^{3+}, respectively. Two possible *ortho* arrangements can exist, but one of them is the same as the *para* arrangement when considering the neighbour unit cells in the crystal lattice. Again, due to the lattice periodicity, the *meta* and *para* arrangements have also two more Mg^{2+} at second neighbours (*meta*) (Fig. 4b, c) taking into account the neighbour unit-cells.

In general, all lattice parameters are similar among the samples of this series. However, sample S18 presents a high value of β for the *ortho* and *para* arrangements and a low value of c in the *meta*, with the $c\sin\beta$ values being similar in all arrangements of S18. All samples with two substitutions of Mg^{2+} in the octahedral sheet show the *meta* arrangement as the most stable (Fig. 5), except in S18. The special behaviour of S18 again is due to the existence of an additional polymorphism caused by the presence of Mg^{2+} as IC. This phenomenon is different than the substitution cation arrangement effect. This aspect will be explored in further studies.

The a and b lattice parameters of the different arrangements are similar within the same sample. The parameter b is slightly higher in S9, with K^+ as IC, than in S3 (Na^+ as IC). Average values of $c\sin\beta$ relative to pyrophyllite, i.e. $c\sin\beta - (c\sin\beta)_{pyro}$, are also plotted as a function of the q/ir of IC (Fig. 6). A negative linear relationship was found and the fitted values of the intercept and the slope are similar to the S13–S17 series.

In samples S3 and S9 all tetrahedral cavities are homogeneously occupied by IC. Hence, only one relative arrangement of octahedral cation with respect to IC is found for each arrangement *ortho*, *meta*, and *para* (Fig. 4). In S15 the IC is divalent and only half of the tetrahedral cavities are occupied. In this sample, only one relative arrangement of octahedral cation with respect to IC is found for each *ortho* and *meta* arrangement (Fig. 5a, b). However, two *para* arrangements are possible: one with the Mg^{2+} pair on the IC (O1) and another with the Mg^{2+} pair on the tetrahedral cavity without IC (O2, Fig. 5c). Nevertheless, the high energy of the *para* arrangement means that the

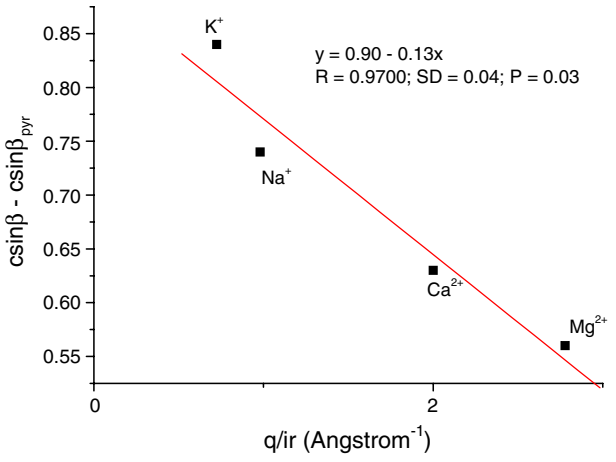

Fig. 3 Relationship between the charge/ionic radius of IC (in $Å^{-1}$, formal charge/ionic radius for octahedral coordination, Shannon 1976) and the increase of *c*sin*β* with respect to pyrophyllite (in Å) for S13, S14, S16, and S17 samples

differences between both *para* arrangements are effectively negligible. We use the O2 arrangements in our calculations. For each sample, no significant lattice parameter difference is detected between the arrangements (Table 3). In all samples of this group, the most stable arrangement is the *meta* arrangement and the least stable is the *ortho* arrangement. Here the energy differences are higher than those derived from IC/tetrahedral or IC/octahedral cation arrangements in previous samples. The *ortho* arrangement has the highest energy due to having the highest polyhedron distortions and the highest repulsive interactions of the negative charge coming from the two $^{VI}Mg^{2+}$ as first neighbours separated by 3.071 Å. This arrangement forms a chain of Mg^{2+} cations along the *a* axis (Figs. 4a, 5a) producing a high charge concentration along this direction and a high distortion in the polyhedron coupling due to the higher ionic radius of Mg^{2+} than that of Al^{3+}; hence this arrangement might be expected to have a low probability of forming within local domains of natural samples. In the *para* arrangements two Mg^{2+} are found as first neighbours separated by 2.953 Å, but the next Mg^{2+} cations are found as second and third neighbours; hence the *para* arrangement has lower energy than the *ortho*. In the *meta* arrangement the Mg^{2+} cations are found only as second neighbours to each other, and hence the *meta* arrangement is the most stable. Average differences of energies between the *ortho* and *meta* arrangements of this series are around 0.6 eV (14 kcal/mol) and the *para* values between 0.2 and 0.3 eV (3 and 6 kcal/mol).

Cation exchange potentials

To analyze the cation arrangement in the octahedral sheet of Al_2Mg_2 samples, the energy of an arrangement can be analyzed in terms of interaction energies (at first, second, third, and forth neighbours) between both cations (*A* and *B* for Al^{3+} and Mg^{2+}, respectively) in the *ortho, meta*, and *para* arrangements in the unit cell, as identified by Sainz-Díaz et al. (2003b):

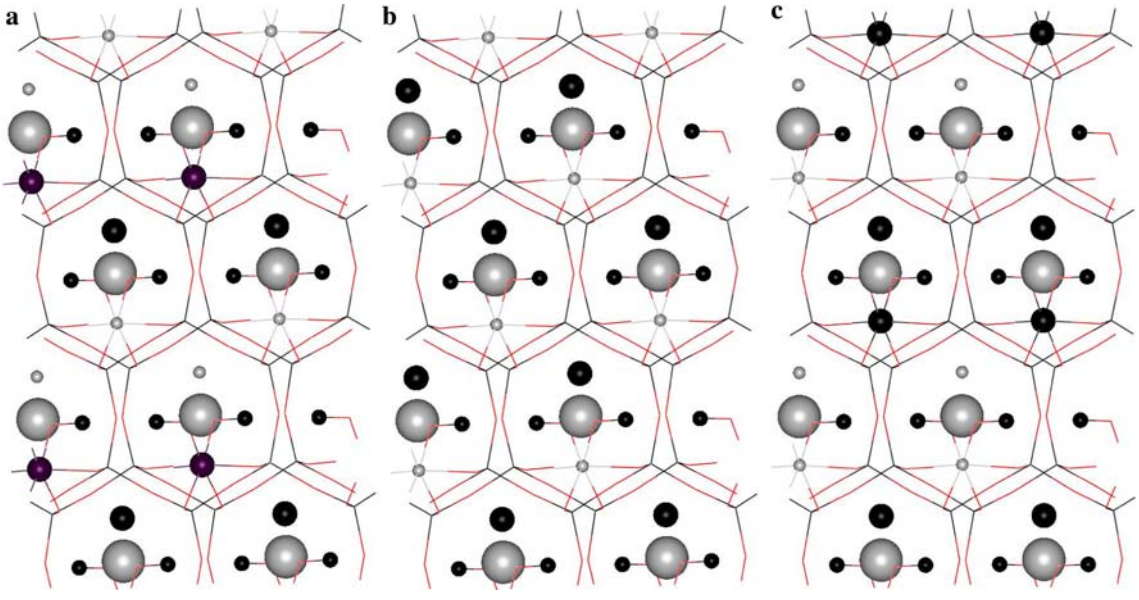

Fig. 4 Cation arrangements, *ortho* (**a**), *meta* (**b**), and *para* (**c**), of the octahedral substitution calculated for S3 and S9. The IC, octahedral substitution, octahedral Al, and H atoms are represented by *big grey*, *medium black*, *small grey*, and *small black balls*, respectively

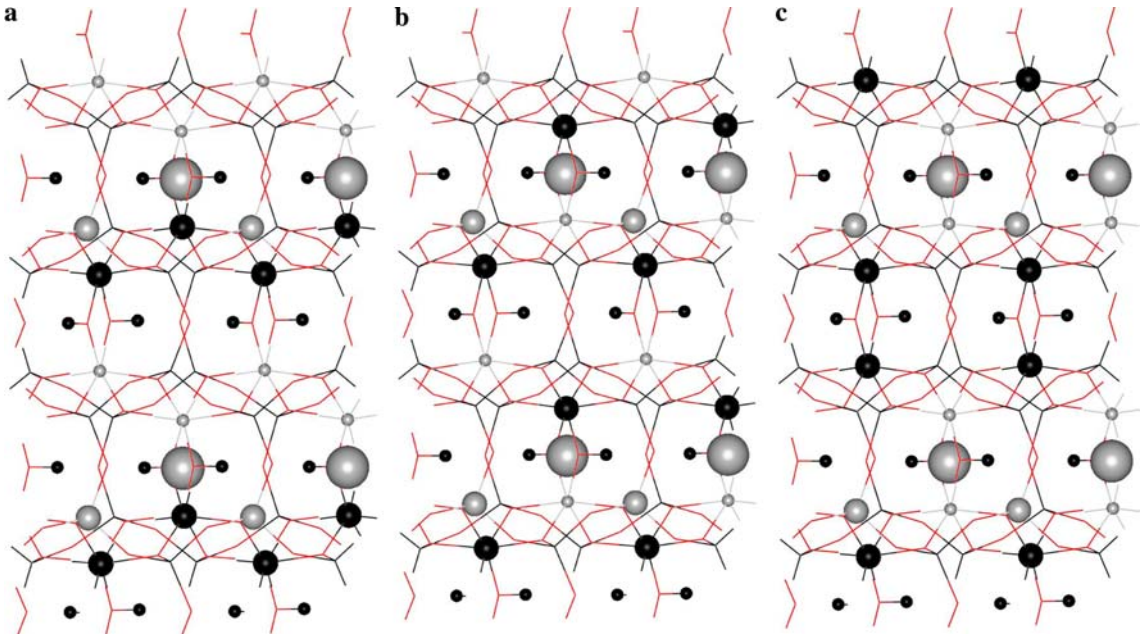

Fig. 5 Relative arrangements, *ortho* (**a**), *meta* (**b**), and *para* (**c**), of the octahedral substitution, calculated for S15 and S18 (without ^{IV}Al substitution), and S2 and S8 with ^{IV}Al substitution in T2 configuration. The octahedral Al and ^{IV}Al cations and IC are represented by *small, medium, and large grey balls*, respectively, and octahedral substitution and H atoms are represented by *medium and small black balls*, respectively. When the octahedral substitutions are one Fe^{3+} and one Mg^{2+} per unit cell without ^{IV}Al substitution, this model represent the S5 and S11 samples

$$E_o = 2(E^1_{AA} + E^1_{BB} + E^1_{AB}) + 2(E^2_{AA} + E^2_{BB} + 4E^2_{AB}) + 6E^3_{AB} + 4(E^4_{AA} + E^4_{BB} + E^4_{AB}) + E_C$$

$$E_m = 6E^1_{AB} + 6E^2_{AA} + 6E^2_{BB} + 6E^3_{AB} + 12E^4_{AB} + E_C$$

$$E_p = E^1_{AA} + E^1_{BB} + 4E^1_{AB} + 2(E^2_{AA} + E^2_{BB} + 4E^2_{AB}) + 3E^3_{AA} + 3E^3_{BB} + 2(E^4_{AA} + E^4_{BB} + E^4_{AB}) + E_C$$

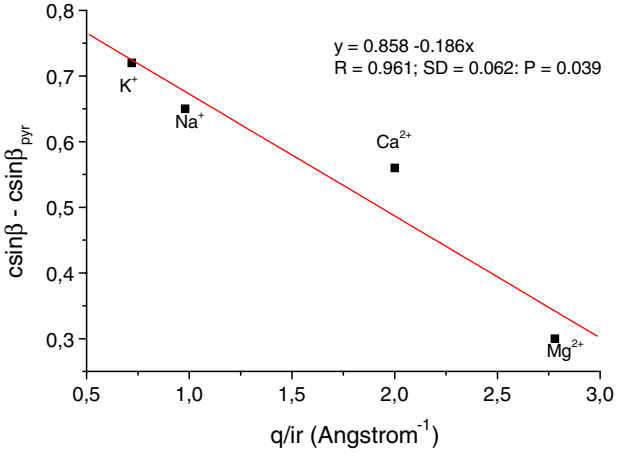

Fig. 6 Relationship between the charge/ionic radius (for octahedral coordination; Shannon 1976) of IC (in $Å^{-1}$) and the increase of $c\sin\beta$ with respect to pyrophyllite (in Å) for octahedral two-substitutions of Mg^{2+} (S3, S9, S15, and S18 samples)

where E^i_{jk} corresponds to the j and k atom interaction energies at ith neighbours (i = 1, 2, 3, 4 account for first, second, third, and fourth neighbours of the cations in the octahedral sheet) and E_C is the constant component of the energy where the contribution of the rest of interactions is included. If we consider that E^3_{jk} and E^4_{jk} are much smaller than E^1_{jk} and E^2_{jk} for qualitative comparisons, we can obtain the following equations:

$$E_o - E_p = E^1_{AA} + E^1_{BB} - 2E^1_{AB} = J^1_{AA}$$

$$\frac{E_o + E_m - 2E_p}{4} = E^2_{AA} + E^2_{BB} - 2E^2_{AB} = J^2_{AA}$$

where J^1_{AA} and J^2_{AA} correspond to the interchange–interaction potential terms that is the energy change for forming two homocationic pairs from two heterocationic pairs, as first and second neighbours, respectively (Bosenick et al. 2001; Palin et al. 2003) (Table 4). The first neighbour terms are much greater than the second neighbour terms. These potentials are consistent with those calculated previously using empirical interatomic potentials and supercells in samples with lower content of Mg, $(Si_{7.7}Al_{0.3})(Al_3Mg)$ (Sainz-Díaz et al. 2003a), albeit slightly smaller. In both cases, these positive values of J's show a mixing tendency for these Al/Mg cations.

Table 4 Exchange potentials of octahedral cations for $Si_8Al_2Mg_2$ samples

Sample	J^2_{AA} (eV)	J^2_{AA} (eV)
S3 (IC = Na^+)	0.3380 (0.652)	0.0270 (0.162)
S9 (IC = K^+)	0.3190 (0.656)	0.0071 (0.168)
S15 (IC = Ca^{2+})	0.4755	0.0833

Comparison with previously calculated values for ($Si_{7.7}Al_{0.3}$)(Al_3Mg) samples in brackets (Sainz-Díaz et al. 2003a)

First and second neighbour terms can be plotted as a function of *q*/ir of IC (Fig. 7) finding positive linear relationships in both cases. The lowest values correspond to the potassium sample, S9, and the highest ones to the calcium sample, S15. Clearly, these cation exchange potentials are not independent of the IC charge/ionic radius, probably because of the different penetrations of the IC in the ditrigonal hole. This effect was not detected in previous investigations (Sainz-Díaz et al. 2003a) on samples with lower substitution of Mg^{2+} and lower interlayer charge than in our studies. Although our exchange potentials are approximate due to neglect of third and fourth neighbours, this result highlights the necessity of further calculations of cation ordering in clays with different IC and cation substitution levels.

Samples with two simultaneous octahedral substitutions of Mg^{2+} and Fe^{3+}

The double substitution in the octahedral sheet may also be one Mg^{2+} and one Fe^{3+} per unit cell, without tetrahedral substitution (samples S5 and S11). The heterogeneity of the substitution means that two arrangements with respect to the IC are possible for *ortho* and *meta* arrangements: one with the Mg^{2+} close to IC O1 (Fig. 4) and the other with the Fe^{3+} close to IC O1. The energy differences between these O1/O2 arrangements are much lower than the differences between *ortho* and *meta*, taking into account the low energy differences observed in S4 and S6. We use the arrangement O1 for Mg^{2+} and O2 for Fe^{3+} cations in our calculations. The arrangement *para* can have two possible arrangements with respect to the IC: one with both substitutions close to IC, O1, and the other with both substitutions close to the (200) plane, O2 (Fig. 4). We use the O2 arrangements in our calculations as in the previous S15 sample. For each sample, no significant lattice parameter differences are detected between the arrangements (Table 3). In both samples the *meta* arrangement is the most stable. The *para* has similar or slightly higher energy than *meta*, whereas the *ortho* is less stable than the *para*. However, the difference of energy between *ortho* and *meta* arrangement is lower than in the two $^{VI}Mg^{2+}$ series, possibly because $^{VI}Fe^{3+}$ does not produce a negative charge in the layer, the repulsive interactions are lower, and the charge distribution is much more disperse than in the previous series.

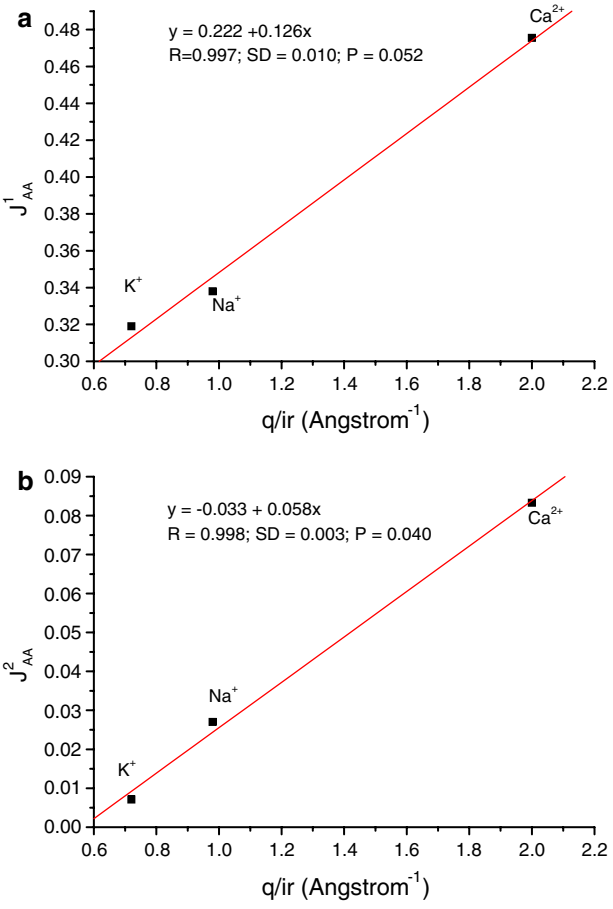

Fig. 7 Cation exchange potentials as first (**a**) and second (**b**) neighbour terms (eV) as a function of the formal charge/ ionic radius

Average values of $csin\beta$ are also a little higher in the potassium (S11) than in the sodium (S5) samples, due to the higher ionic radius of the K^+, and the slope of the linear relationship of $[csin\beta - (csin\beta)_{pyro}]$ with respect to *q*/ir is similar to that of other previous series.

Samples with two simultaneous octahedral substitutions of Fe^{3+}

Two Fe^{3+} cations can also substitute for two Al^{3+} in the octahedral sheet within one unit cell (samples S2 and S8). Here no octahedral charge is generated and there is one $^{IV}Al^{3+}$ per unit cell in T2 position (Fig. 5). We use the O2 positions for the *para* arrangements of Fe^{3+} substitutions in our calculations. In all samples of this group, the most stable arrangement is the *ortho*

arrangement and the least stable is the *meta* arrangement (Fig. 5). The energy differences are lower than the previous two-substituted octahedral series, but much higher than those derived from IC/tetrahedral or IC/octahedral substitution arrangements in previous samples. Nevertheless, the energy difference of the arrangement with Fe^{3+} cations in *ortho* arrangements with respect to *meta* arrangement is only 0.22 eV (5 kcal/mol).

No significant differences in the lattice parameters are observed between the arrangements for each sample. The sample S8, with K^+ as IC, shows slightly higher values of *a*, *b*, and *c* parameters than S2 (with Na^+ as IC), as in samples shown above (Table 3). The average values of $csin\beta$ are also larger in the S8 than in the S2 series. The slope of the linear relationship of $[csin\beta - (csin\beta)_{pyro}]$ with respect to *q*/ir is –0.41, larger than that of the previous slope, possibly because in this series the charges only come from one of the tetrahedral sheets and the IC cations do not penetrate in the ditrigonal hole.

Discussion

The agreement between calculated and experimental values of the lattice parameters for the systems studied supports the use of these quantum–mechanical calculations for the study of phyllosilicates. In addition, the practical ability to use different isomorphic cation substitutions in both tetrahedral and octahedral sheets and several IC confirms the utility of this theoretical approach to explore realistic dioctahedral 2:1 phyllosilicates.

The importance of the *q*/ir ratio of the IC is highlighted in the following items: (1) penetration of the electronic shell of IC in the tetrahedral ditrigonal hole; (2) opening of the interlayer space; (3) interaction with the octahedral cations; (4) the exchange interaction potential terms at first and second neighbours; and (5) the high *q*/ir value of Mg^{2+} as IC produces important relative energy differences of the different octahedral arrangements, and in the crystal structure, producing different polymorphs.

The larger penetration can come by means of a tilting of tetrahedra and a change in the Si–O–Si and O–Si–O angles of tetrahedral hole, changing the coordination number (CN) of the IC with respect to the tetrahedral oxygens. Taking into account the symmetry of the tetrahedral hole, two coordination structures can exist: octahedral and 12-fold coordinations. The ionic radius of both Na^+ and K^+ in octahedral coordination are less than those in 12-fold coordination (Shannon 1976), in such a way that a different ionic radius of the IC could exist as a consequence of a change in the CN of each IC. Therefore, Na^+ in 12-fold coordination will have an ionic radius similar to that of K^+ in octahedral coordination. Thus, the interlayer space with K^+ will be shorter than that corresponding to that expected if the ionic radius is associated with equal CN of both IC. Another reason for this phenomenon could be the larger overlapping of the most external orbitals of the larger IC with the lone pairs of the basal oxygens inside the ditrigonal hole, without any change in the angles of the tetrahedra. Possibly a mixture of both effects should occur.

The energy of the different relative arrangements of cations in our samples indicates that the interactions between IC and tetrahedral cations, and those between IC and octahedral cations are much weaker than those between octahedral cations or those between octahedral and tetrahedral cations. This is consistent with previous calculations based on empirical potentials and Monte Carlo (MC) simulations (Palin et al. 2001; Sainz-Díaz et al. 2003a).

The relative arrangement of $^{IV}Al^{3+}$ with respect to the octahedral Mg^{2+} tends to be separated, with the O2T2a arrangement being the most stable (S13, S14, S16, and S17 in Table 2). This means that the tetrahedral and octahedral charge is more likely dispersed than concentrated. This is consistent with the experimental tendency of dispersion for $^{IV}Al^{3+}$ in tetrahedral sheets (Herrero et al. 1987) and for Mg^{2+} in octahedral sheets (Sainz-Díaz et al. 2001a). However, previous studies based on empirical potentials and MC simulations on phengite found a stable ordered cation arrangement where ^{IV}Al and Mg^{2+} are close (Palin et al. 2003). This discrepancy can be due to the assumptions of transferability of the cation exchange potentials taken in the previous work of phengite. Nevertheless, we propose to explore more deeply the simultaneous relative ordering of cations in the three sheets: tetrahedral, octahedral, and interlayer space.

With respect to the octahedral cation arrangement, our calculations match the experimental cation arrangement of Mg^{2+} and Fe^{3+} in the octahedral sheet of clays. The dispersion tendency of Mg^{2+} and the clustering tendency of Fe^{3+} cations in the octahedral sheet are reproduced theoretically. The energy that controls the dispersion of Mg is significantly higher than that related with the segregation of Fe according to our previous calculations using empirical potentials (Sainz-Díaz et al. 2003b). Our calculations are in accord with experimental results which is easier to find small clusters of Fe than MgMg pairs in clay minerals (Cuadros et al. 1999).

In the FeMg systems, the most stable arrangement is the *meta* one, where Fe^{3+} and Mg^{2+} are dispersed, according to previous MC simulations of FeMg systems for clays (Sainz-Díaz et al. 2003a). Nevertheless, the energy difference with the *para* arrangement is not high, indicating that small clusters of FeMg can be detected in these minerals.

Acknowledgments Authors are thankful to E. Artacho, J. M. Soler, and O. Paz for their useful discussions about SIESTA, A. R. Oganov for his comments, exchange program Royal Society of United Kingdom/Consejo Superior de Investigaciones Científicas (CSIC) of Spain, the ''Centro Técnico de Informática'' of CSIC, ''Centro de Supercomputación de Galicia'' (CESGA), and the ''Centro de Supercomputación de la Universidad de Granada'' for allowing the use of its computational facilities. E. Escamilla-Roa is thankful to Agencia Española de Cooperación Internacional (AECI), University of Granada and the BTE2000-1146-CO2-01 grant for financial support. This work was supported by Spanish Ministerio de Educación y Ciencia (MEC) and European FEDER grants BTE2002-03838 and PPQ2004-04648 grants.

References

Artacho E, Sánchez-Portal D, Ordejón P, García A, Soler JM (1999) Linear-scaling ab-initio calculations for large and complex systems. Phys Stat Sol 215:809–817

Bachelet GB, Schluter M (1982) Relativistic norm-conserving pseudopotentials. Phys Rev B25:2103–2108

Besson G, Drits VA, Daynyak LG, Smoliar BB (1987) Analysis of cation distribution in dioctahedral micaceous minerals on the basis of IR spectroscopy data. Clay Miner 22:465–478

Bosenick A, Dove MT, Myers ER, Palin EJ, Sainz-Díaz CI, Guiton B, Warren MC, Craig MS, Redfern SAT (2001) Computational methods for the study of energies of cation distributions: applications to cation-ordering phase transitions and solid solutions. Mineral Mag 65:197–223

Cuadros J, Sainz-Díaz CI, Ramírez R, Hernández-Laguna A (1999) Analysis of Fe segregation in the octahedral sheet of bentonitic illite–smectite by means of FT-IR, ^{27}Al MAS NMR and Reverse Monte Carlo simulations. Am J Sci 299:289–308

Drits VA, Dianyak LG, Muller F, Besson G, Manceau A (1997) Isomorphous cation distribution in celadonites, glauconites and Fe-illites determined by infrared, Mösbauer and EXAFS spectroscopies. Clay Miner 32:153–179

Giese RF Jr (1979) Hydroxyl orientations in 2:1 phillosilicates. Clays Clay Miner 27:213–223

Güven N (1988) Smectites. In: Bailey SW (ed) Hydrous phyllosilicates (exclusive of micas). Reviews in Mineralogy, vol. 19. Mineralogical Society of America, Washington, p 497–561

Herrero CP, Sanz J (1991) Short-range order of the Si, Al distribution in layer silicates. J Phys Chem Solids 52:1129–1135

Herrero CP, Gregorkiewitz M, Sanz J, Serratosa JM (1987) ^{29}Si MAS–NMR spectroscopy of mica-type silicates: observed and predicted distribution of tetrahedral Al–Si. Phys Chem Miner 15:84–90

Kleinman L, Bylander DM (1982) Efficacious form for model pseudopotentials. Phys Rev Lett 48:1425–1428

Krauskopf KB (1991) Radioactive waste disposal and geology. Chapman and Hall

Louie SG, Froyen S, Cohen ML (1982) Nonlinear ionic pseudopotentials in spin-density-functional calculations. Phys Rev B26:1738–1742

Meunier A (2005) Clays. Springer, Berlin Heidelberg New York

Morris HD, Bank S, Ellis PD (1990) ^{27}Al NMR spectroscopy of iron-bearing montmorillonite clays. J Phys Chem 94:3121–3129

Muller F, Besson G, Manceau A, Drits VA (1997) Distribution of isomorphous cations within octahedral sheets in montmorillonite from Camp-Bertaux. Phys Chem Miner 24:159–166

Palin EJ, Dove MT, Redfern SAT, Bosenick A, Sainz-Díaz CI, Warren MC (2001) Computational study of tetrahedral Al–Si ordering in muscovite. Phys Chem Miner 28:534–544

Palin EJ, Dove MT, Redfern SAT, Sainz-Díaz CI (2003) Computational study of tetrahedral Al–Si and octahedral Al–Mg ordering in phengite. Phys Chem Miner 30:293–304

Perdew JP, Burke K, Ernzerhof M (1996) Generalized gradient approximation made simple. Phys Rev Lett 77:3865–3868

Rosso KM, Rustad JR, Bylaska EJ (2001) The exchange in muscovita interlayer: an ab inio treatment, Clays Clay Miner 49:500–513

Sainz-Díaz CI, Cuadros J, Hernández-Laguna A (2001a) Cation distribution in the octahedral sheet of dioctahedral 2:1 phyllosilicates by using inverse Monte Carlo methods. Phys Chem Miner 28:445–454

Sainz-Díaz CI, Hernández-Laguna A, Dove MT (2001b) Modelling of dioctahedral 2:1 phyllosilicates by means of transferable empirical potentials. Phys Chem Miner 28:130–141

Sainz-Díaz CI, Timón V, Botella V, Artacho E, Hernández-Laguna A (2002) Quantum mechanical calculations of dioctahedral 2:1 phyllosilicates: effect of the octahedral cation distribution in pyrophyllite, illite and smectite. Am Miner 87:958–965

Sainz-Díaz CI, Palin EJ, Hernández-Laguna A, Dove MT (2003a) Octahedral cation ordering of illite and smectite. Theoretical exchange potential determination and Monte Carlo simulations. Phys Chem Miner 30:382–392

Sainz-Díaz CI, Palin EJ, Dove MT, Hernández-Laguna A (2003b) Monte Carlo simulations of ordering of Al, Fe, and Mg cations in the octahedral sheet of smectites and illites. Am Miner 88:1033–1045

Sainz-Díaz CI, Escamilla-Roa E, Hernández-Laguna A (2005) Quantum mechanical calculations of trans-vacant and cis-vacant polymorphism in dioctahedral 2:1 phyllosilicates. Am Miner 90:1827–1834

Sato T, Watanabe T, Otsuka R (1992) Effects of layer charge, charge location and energy charge on expansion properties of dioctahedral smectites. Clays Clay Miner 40:103–113

Schroeder PA (1993) A chemical, XRD, and ^{27}Al MAS NMR investigation of Miocene Gulf Coast shales with application to understanding illite-smectite crystal-chemistry. Clays Clay Miner 41:668–679

Shannon RD (1976) Revised effective ionic radii and systematic studies of interatomic distances in halides and chalcogenides. Acta Cryst A32:751–767

Soler JM, Artacho E, Gale JD, Garcia A, Junquera J, Ordejon P, Sanchez-Portal D (2002) The SIESTA method for ab initio order-N materials simulation. J Phys Cond Mat 14:2745–2779

Troullier N, Martins JL (1991) Efficient pseudopotentials in spin-density-functional calculations. Phys Rev B43:1993–2006

Tsipursky SI, Drits VA (1984) The distribution of octahedral cations in the 2:1 layers of dioctahedral smectites studied by oblique-texture electron diffraction. Clay Miner 19:177–193

Velde B, Espitalié J (1989) Comparison of kerogen maturation and illite/smectite composition in diagenesis. J Petrol Geol 12:103–110